PREPRINT

Synthesis of Manganese Oxide Nanoparticles in Premixed Stagnation Flames

Shruthi Dasappa, Joaquin Camacho

Mechanical Engineering Department, San Diego State University, San Diego, California 92182, USA

Abstract

Synthesis of manganese oxide nanoparticles was carried out in premixed stagnation flames. The deposition surface was stationary to enable rigorous comparison to flame structure computations using pseudo one-dimensional and full two-dimensional calculations. The pseudo one-dimensional assumption taken by OPPDIF to calculate the flame structure performs reasonably well for the narrow aspect ratio stagnation flow currently studied. Agreement between the measured flame position and both computational methods was within 0.25 cm. The variation in manganese oxidation state in the products observed here is shown to be caused by competing oxidation and particle nucleation processes. Complimentary experimental and modeling studies of flame synthesis were carried out under well-defined boundary conditions to examine this competition. Manganese oxide products having II, II,III, III and IV valence were observed depending on the flame conditions. Unlike iron oxide and titanium oxide systems, complete oxidation to MnO_2 is only observed for the most oxidizing growth conditions. The first observation of phase pure MnO by flame synthesis is reported here. Manipulation of the balance between manganese oxidation and particle nucleation through control of the time-temperature-oxygen history may enable selective synthesis of manganese oxide nanoparticles with tailored morphology and oxidation state.

Keywords:

Manganese Oxide, Nanoparticle, Flame Synthesis, Premixed Flame, Chemical Vapor Deposition

1. Introduction

Strained premixed laminar flames are important tools for understanding fundamental combustion behavior [1]. Beyond extinction [2] and laminar flame speed [3], the premixed stagnation flame configuration has also been used in material synthesis for some time [4, 5]. In the current study, manganese oxide nanoparticles are synthesized in premixed stagnation flames with well-characterized flame structure and boundary conditions. Competing oxidation and growth mechanisms for manganese oxide will be examined in terms of systematic variation of the in-flame temperature-time-oxygen history.

Manganese oxide nano-materials have been incorporated into many promising technologies including energy storage materials [6, 7] and catalysts (see e.g., NOx [8], Water Oxidation [9]). Flame made manganese oxide nano-materials, mostly produced by flame spray pyrolysis [10, 11], have been reported for a variety of applications. Manganese oxide nanoparticles produced by flame stabilized on a rotating surface (FSRS) was reported previously [12] and it was observed that either Mn_3O_4, Mn_2O_3 or MnO_2 are formed depending on growth conditions in the premixed flame. This is in contrast to many titanium oxide and iron oxide studies in premixed flames where full oxidation to TiO2 and Fe_2O_3 is reported. There are notable exceptions such as a recent report of TiO_2-II formation in fuel rich FSRS conditions [13]. In the current study, synthesis of manganese oxide nanoparticles in premixed stagnation flames will be carried out on a stationary deposition surface to further examine competing processes leading to the final oxide product.

A complimentary modeling and experimental approach will be taken in terms of studying the flame structure of the strained premixed laminar flame. Solutions obtained using the pseudo one dimensional (self-similar) formulation will be compared to a separate computation of the two-dimensional axis-symmetric flame structure. As first outlined by Kee [4], computation of the flame structure using the similarity formulation could enable efficient yet powerful process design for material synthesis in strained laminar flames. The similarity scaling of a linear dependence on r for radial velocity is most accurate for domains with a wide burner to stagnation aspect ratio [14, 15]. In the current work, the aspect ratio of the burner to stagnation is relatively narrow as it is closer to some

CVD geometries [16]. The comparison between one and two-dimensional flame computations will provide insight into efficient flame structure calculation for the narrow aspect ratio domain and relatively large flame standoff distance considered.

2. Computational Methods

Premixed stagnation flames on a stationary surface are modeled here using both a pseudo one-dimensional model and a full two-dimensional axisymmetric computation. The flame computations do not include particle precursor, nor do they consider nanoparticle synthesis processes in the flame. Rather, the flame structure resulting from the base ethylene-oxygen-argon mixture is calculated. An experimental comparison between flames with and without precursor doping is carried out below to assess the range, if any, for neglecting role of the Mn oxide precursor on the flame structure. An objective of the study is to determine the accuracy of using the pseudo one-dimensional computation for material synthesis processes having geometry at the limits of the self-similar range.

The one-dimensional solution was obtained using OPPDIF [17] modified to include CO_2 and H_2O radiation [18]. The boundary conditions include the measured temperatures at the boundaries and the inlet flow rates. Plug flow (zero radial velocity) is assumed at the nozzle and diffusion of species is allowed into the nozzle boundary. The axial, radial and diffusive velocities are zero at the stagnation surface and the zero diffusive velocity for each species is the result of counteracting Fickian and thermal diffusion processes. Windward differencing, the multicomponent transport formulation and thermal diffusion was considered within the Sandia CHEMKIN framework [19]. The two-dimensional axisymmetric computation also used CHEMKIN to evaluate the chemical kinetic, thermal and transport aspects of the reacting flow. The reaction kinetic model considered for both computations was USC Mech II [20], which has been shown to calculate heat release rates and premixed stagnation flame structure more accurately than other foundational mechanisms [21, 22].

The two-dimensional axisymmetric computation was carried out on ANSYS Workbench (v.19.2) incorporating Fluent and Chemkin. The governing equations for continuity, momentum, energy and species conservation were solved in the axial and radial directions using CHEMKIN-CFD invoked through Fluent. The axisymmetric domain is defined along the axis of the burner nozzle and the width

and height of the domain is 7.0 and 2.54 cm, respectively, for all flames. The domain is a simple projection of flame configuration without consideration of confinement or entrainment effects. The nozzle is considered a boundary of the domain as a 0.5 cm slit normal to the centerline (for the 1 cm diameter nozzle). The N_2 sheath flow channel is a 0.2 cm opening adjacent to the nozzle opening. The mesh is 40800 cells mostly concentrated within 4 cm of the axis (99%). The side faces of the domain are pressure outlets, the stagnation surface face is specified as a wall boundary. The nozzle and sheath openings are set as velocity inlets. The Fluent viscosity model is set to laminar and the Chemkin mechanism is uploaded into the species-transport module. Radiation is not considered but thermal diffusion and multicomponent transport are. The initial guess for iterations is based on the OPPDIF solution for temperature and flame position. During initialization, the temperature, O, H and OH concentrations are applied to a thin region on the mesh where OPPDIF predicts the flame position to be.

For ease of computation, the two-dimensional solution was only obtained for a limited set of flames and OPPDIF was relied upon to determine the temperature-time-oxygen history for particle synthesis. The performance of both computations is assessed in terms of comparison to experimentally measured flame position as discussed below. An objective of the current study is to show that the pseudo one-dimensional formulation is an efficient process design tool for stagnation flames. Manganese oxide has been produced in premixed flames with a variety of oxidation states [12] and characterization of the flame structure is important for elucidating the competing processes. The current synthesis process is relatively one-dimensional as there is no radial species. The particle time, t_p , is considered to be the time for a Langrangian particle to traverse the location of the flame (considered as position where the temperature inflects sharply upwards) to the location of the stagnation surface. The particle time is considered to approximate the time for MMT precursor breakdown, Mn oxidation and particle nucleation / growth to occur before deposition. Examination of the relationship between the oxide product properties and the synthesis flame structure is expected to shed light on the competing oxidation, nucleation and growth time scales.

3. Experimental Methods

Flame synthesis of manganese oxide nanoparticles is carried out in premixed stagnation flames with subsequent deposition onto a stationary surface. This is a vapor-fed process in which methylcyclopentadienyl manganese tricarbonyl (MMT, Sigma-Aldrich) liquid precursor is mixed with the unburned mixture and vaporized in the fuel line. In the flame, MMT decomposes, burns and the oxide product nucleates to form an aerosol. The experimental setup is similar to the carbon deposition experiments reported previously [23]. A new contraction nozzle was designed with inner contours taken from Bergthorson [24] and a relatively broad rim to minimize flame flashback. The aluminum nozzle has a nozzle diameter D = 1.0 cm and the wall thickness is 0.2 cm at the nozzle exit. A shroud of nitrogen issuing from a concentric channel surrounds the main mixture flow. Manganese oxide products were deposited from the flame onto a stationary substrate with the nozzle-to-stagnation separation kept at L = 2.54 cm for all experiments. Fine wire, type K thermocouples were used to measure temperature of the unburned gas (nozzle boundary temperature) and the temperature at the deposition surface (stagnation boundary temperature).

Premixed stagnation flames provide high-temperature synthesis conditions with radial uniformity in thermal and chemical profiles [4, 5]. In the current study, the flame structure is manipulated to give flame synthesis conditions with a desired temperature-time-oxygen history for particle growth. This can be achieved by proper balancing of the flow momentum and flame reactivity. For example, the strain rate was systematically decreased, in previous work, for a given unburned mixture to observe soot formation at increasing growth time [21]. The flame position will be measured by analyzing the flame projection captured by DSLR camera as described previously [21, 23].

Table 1. Summary of flame synthesis conditions

Flame	ϕ	X_{Ar}	$T_{f,max}$ (K)	$t_p(L)$ (ms)	MMT (ppm)	Velocity, v_o (cm/s)
A1	0.4	0.46	2600	4	200	335
A2	0.4	0.46	2600	4	300	335
A3	0.4	0.46	2600	4	500	335
B1	0.4	0.52	2510	4	100	301
B2	0.4	0.46	2600	4	100	335
B3	0.4	0.52	2510	4	200	301
B4	0.4	0.46	2600	4	200	335
B5	0.4	0.62	2340	7	500	252
B6	0.4	0.56	2450	6	500	290
B7	0.4	0.52	2510	4	500	301
B8	0.4	0.46	2600	4	500	335
C1	0.4	0.46	2600	4	100	335
C2	0.5	0.61	2560	5	100	299
C3	0.6	0.67	2590	5	100	305
C4	0.8	0.72	2620	5	100	316
D1	1.2	0.81	2390	7	200	267
D2	1.3	0.79	2480	6	200	279
D3	1.4	0.79	2400	7	200	269
D4	1.5	0.78	2390	6	200	279

Premixed ethylene-oxygen-argon laminar flames doped with MMT precursor will be studied in the current work. A summary of the flame conditions studied is summarized in Table 1 in terms of experimental sets defined by flame temperature, time and oxygen environment. A more detailed table is included in the supplemental material. Design of the experimental flame synthesis conditions was based on OPPDIF computations of the flame structure. Comparisons to experimental measurements of flame position and the two-dimensional computation will provide insight into the accuracy of OPPDIF for this nozzle-to-surface separation. Another assumption is that MMT does not perturb the flame structure at the doping level considered here. With this is mind, the flame temperature, oxygen and time profiles assigned to the experimental flames are determined by OPPDIF using measured boundary conditions.

The first set of experiments, labeled as the A series of flames, examines manganese oxide nanoparticle formation in flames having $\phi = 0.4$, $T_{f,max} = 2600$ K and $t_p = 4$ ms at increasing levels of MMT loading (Flames A1-A3). As reported previously [12], the competition between manganese oxidation and particle growth is expected to be affected by precursor concentration for a given flame condition. The nanoparticle products are expected to form under the same temperature-time-oxygen

history while undergoing different rates of particle growth. Particle nucleation is expected to occur fastest in flame A3 which would indicate that oxidation of manganese in the fluid phase stops sooner at higher precursor doping. Of interest is to determine whether this relatively short time for fluid oxidation explains the lower manganese oxidation states observed previously for high precursor loading.

The fuel lean condition (ϕ = 0.4) is used again in experiment B to observe manganese oxide formation for a series of increasing flame temperature conditions (2340 K < $T_{f,max}$ < 2600 K) all at comparable particle time, t_p (Flames B1-B8). In principle, kinetic parameters could be obtained by observing the onset of manganese oxide products as a function of time and temperature. A series of flames with comparable temperature and particle time is used in experiment C to examine the role of gas-phase oxygen (0.4 < ϕ < 0.8). Low MMT loading (100 ppm) to examine the range where full oxidation to MnO_2 is limited by post-flame oxygen concentration. Experiment D further explores oxygen concentration effects in oxygen lean growth conditions. Th series of flames having 1.2 < ϕ < 1.5 is expected to produce lower oxidation state of manganese oxide.

Manganese oxide films deposited from the stagnation flame were characterized by off-line Raman spectroscopy, X-ray diffraction (XRD) and transmission electron microscopy (TEM). A Thermo DXR2 Raman Microscope with a 532 nm excitation source was used for spectra having Raman shifts spanning 300 to 3000 cm^{-1} . The laser was focused under a 50x objective at 1 mW power. XRD measurements were carried out on a PANalytical X'pert Pro diffractometer equipped with a Cu X-ray tube operating at 45 kV and 40 mA. Counts were made for 1.5 sec for each 0.02 increment for 20 < 2θ < 60. The samples are transferred from the aluminum deposition substrate to glass for XRD analysis to avoid diffraction from aluminum. A FEC Tecnai 12 Transmission Electron Microscope is employed with a Teitz 214 high resolution bottom mounted digital camera.

The objective of the experiments is to examine the competition between the time scales of manganese oxidation and particle growth. A hypothesis is that the nucleation of particles effectively quenches manganese oxidation because solid phase oxidation is much slower than oxidation of fluid phase manganese. The well-characterized boundary conditions enable complimentary studies of flame

synthesis where this hypothesis could be tested using analytical or numerical modeling [4, 15]. This complimentary approach enables determination of thermodynamic and kinetic parameters that could be generalized for any synthesis process.

4. Results and Discussion

Modeling tools are used here to design flame conditions with desired temperature-time-oxygen histories in the post-flame region. Computed flame structures, neglecting precursor doping, are the basis for determining the particle growth environment in the current work. The comparison between experimental and computed flame structure is shown in Fig. 1 in terms of recorded flame images and computed 2D contours. Recorded flame images were analyzed to determine the flame standoff distance and results for flames (2340 K < $T_{f,max}$ < 2600 K, B5-B8) compared to the computed flame structure are presented in supplementary material. The MMT doped flame shows a post-flame region illuminated by excited Mn oxide precursors. The base flame is stabilized in roughly the same position as the precursor doped flame. The position of the 100 ppm of MMT flame is slightly closer to the nozzle boundary which may indicate that this mixture is more reactive than the base flame. This effect may be caused by catalytic behavior of manganese or a mixture closer to stoichiometric. The two-dimensional computation of the flame structure shows reasonable agreement to the images in terms of the computed temperature contour. There are instabilities and influences from the environment which result in broadening of the flame position observed in the flame images. A small degree of chemiluminescence appears in a broad region surrounding the MMT doped flame which is caused by minor flickering and oscillation instabilities.

A comparison in terms of the flame structure at the centerline is shown in Fig. 2. Measured pixel intensity at the centerline is compared to calculated temperature and CH profiles. The doped flame pixel intensity maps out the region of high-temperature emission from manganese oxide precursors. Without precursor, the excited combustion intermediates are the only source of illumination and a rough comparison of the measured pixel intensity to computed CH profiles is shown at the inset. Assuming that the measured pixel intensity is due to CH, the discrepancy in measured and computed flame position is 0.25 cm compared to ANSYS. Comparison between the measured pixel intensity

and the steep temperature gradient computed by OPPDIF shows good, fortuitous or not, agreement. The flame temperature gradient predicted by the ANSYS 2D solution lies within 0.15 cm of the doped flame pixel intensity. Both OPPDIF and ANSYS 2D compile USC Mech II in the Chemkin framework with the accompanying thermodynamic and transport models. One difference in the computation is that radiation effects are ignored in the ANSYS workbench and this could explain the higher temperature predicted in the two-dimensional computation.

Many two-dimensional flame modeling studies have been carried out to evaluate the optimal counterflow conditions to achieve self-similar conditions. A common focus is the inlet boundary in which plug-flow is important for accurately extrapolating the laminar flame speed from low-strain premixed flames [25]. More careful treatment of the boundary flow profile could extend the range of the self-similar computation for flame extinction and [2] for flames outside of the mixing layer [26]. A typical velocity and particle time profile is shown in Fig. 3 for both the self-similar (OPPDIF) and two-dimensional (ANSYS) computation. The particle time is only defined in the post-flame region thus the total velocity shown in Fig. 3 is the convective velocity plus particle thermophoresis velocity added in the post-flame. Higher predicted flame temperature for the two-dimensional calculation has been reported [26, 27] and radial momentum and energy equation considerations were shown to become significant for large aspect ratio stagnation configurations [26, 28]. These radial uncertainties will be investigated in future work. Overall, the flame position is predicted reasonably well for OPPDIF and ANSYS two-dimensional methods. This comparison indicates that the self-similar assumption taken by OPPDIF provides a fast and accurate computation of the flame structure for a robust range of premixed stagnation flame conditions.

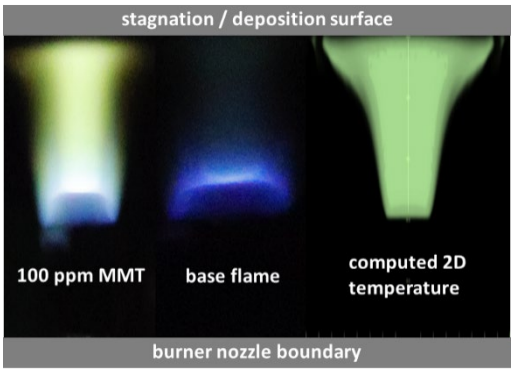

Figure 1. Comparison between measured and computed flame position in terms of flame images (left) and 2D temperature contour computed with ANSYS (right).

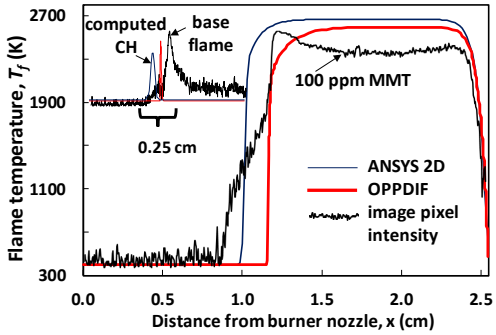

Figure 2. Comparison between measured and computed flame centerline profiles. Computed temperature and CH profiles (inset) is compared to measured pixel intensity at the flame centerline for the base flame (inset) and an MMT doped flame.

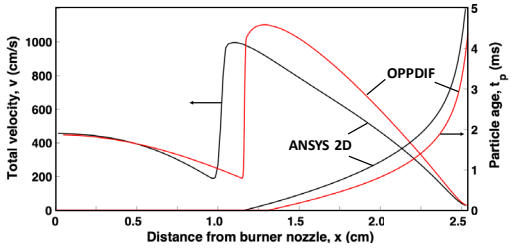

Figure 3. Computed velocity and particle time profiles using OPPDIF and ANSYS 2D calculations.

The A series of experiments was designed to show oxidation limited by competing particle nucleation processes. Flame A (ϕ = 0.4, $T_{f,max}$ = 2600 K and t_p = 4 ms) was examined with 200 , 300 and 500 ppm levels of MMT loading. A summary of the manganese oxide products in terms of XRD, Raman and TEM characterization is shown in Fig. 4. Particle sizing by analysis of the TEM images in ImageJ indicates that the size of particles ranges roughly from 5 -7 nm for the conditions studied. Faint evidence of lattice fringes were observed in the 300 ppm doping case. As expected, X-ray diffraction is not strong for these relatively disordered and ultrafine particles. The most prominent

faces were observed on the 500 ppm case as (222) and (444) attributed to Mn_2O_3. Faint evidence of MnO_2 peaks appears as (101) and (110) in the lower ppm loading cases. Examination of short range order by Raman spectroscopy shows a more clear evolution at increasing particle loading. The A_{1g} breathing mode of Mn oxide octahedra is observed at 650 cm^{-1} for 200 and 500 ppm and this is a characteristic of Mn_3O_4. Several studies attribute this to known thermal decomposition behavior of Mn_2O_3 under laser power [29], [30]. The flame synthesis origin of the manganese oxide may have caused this high-temperature feature to persist in the product structure rather than artifacts from the laser (1 mW). The Mn-O stretch mode is observed at 680 cm^{-1} for the 300 and 500 ppm cases which corresponds to Mn_2O_3 [29]. The Raman spectra of the 200 ppm loading case shows a clear departure in that the dominant mode A_{1g} is no longer present. Instead, broad A_g modes are observed above 600 cm^{-1} and these have been attributed to disordered MnO_2 structures [30]. The manganese oxide products in series A indicate that particle nucleation processes compete with oxidation. Incomplete oxidation products may be observed because particle nucleation occurred before oxidation to MnO_2 is completed. Oxidation may be effectively quenched after a Mn oxide cluster nucleates into the solid phase.

Oxidation rates of manganese are explored further in the experiment B series of flames. A summary of products formed is shown in Fig. 5 for a range of flame temperature (2340 K < $T_{f,max}$ < 2600 K). The computed flame structure based on the pseudo one-dimensional formulation indicates that particles synthesis will occur across a range of flame temperature at comparable growth times. The Raman spectra shows the structure of oxide formed depends strongly on the temperature and particle loading conditions. Features of Mn_2O_3 products are observed for 500 ppm MMT loading at all temperature conditions. This is contrasted to the spectra for the lower ppm conditions of the same flames. Manganese oxides forming in the 100 and 200 ppm loading cases have Raman features corresponding to MnO_2 structures with a range of disordered structure [30]. Assuming the computed particle time is the characteristic reaction time with dilute precursor conditions, the conversion of MMT to MnO_2 structures in premixed stagnation flames has first order activation energy on the order of 30 kJ/mol. Full oxidation to MnO_2 only occurs when the oxidation rate is enhanced by higher

temperatures or dilute precursor conditions. In the flames currently studied, flame temperature has a weak effect on the products observed when particle nucleation is fast. Oxidation is hindered by the nucleation of solid phase manganese oxide. Dilution of the precursor delays the onset of nucleation for a given flame. When particle nucleation is surpressed (slower growth *via* dilution), a more diverse set of oxide products is observed depending on the time-temperature-oxygen history.

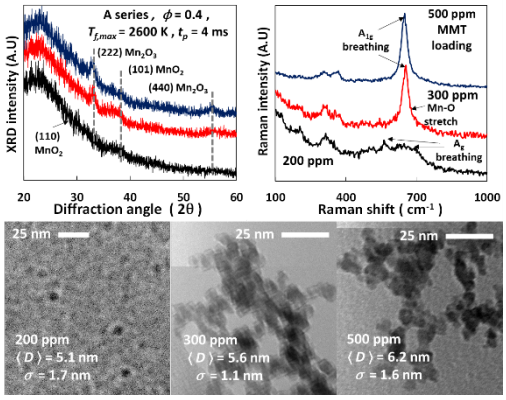

Figure 4. Summary of manganese oxides formed in experiment A series of flames. XRD patterns (top-left) , Raman spectra (top-right) and TEM images (bottom row) are shown for increasing particle precursor loading.

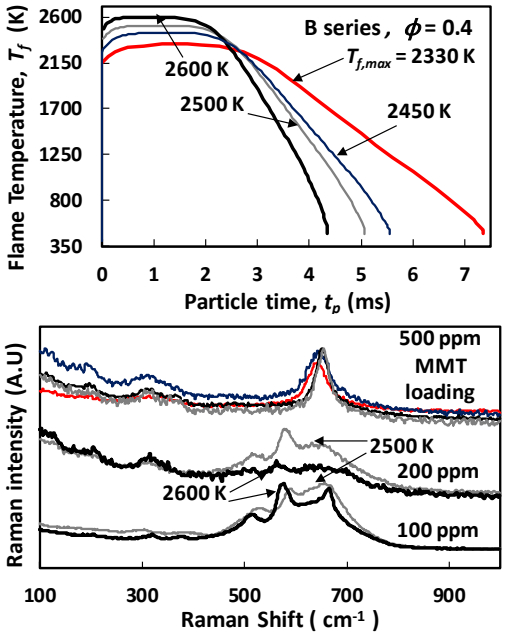

Figure 5. Summary of manganese oxides formed in experiment B series of flames. Computed (OPPDIF) temperature-time history for B series (2330 K < $T_{f,max}$ < 2600 K, top panel) and Raman spectra of products formed over the series of flame temperature and precursor loading (bottom panel).

Oxidation processes are further examined for the low precursor loading (100 ppm) condition in series C experiments ($0.4 < \phi < 0.8$). The variety of peaks observed from 500-700 cm^{-1} have been attributed to MnO_2 with various degrees of pyrolusite (order) [30]. At low oxygen conditions, the Raman spectra of the products formed begins to show features of Mn_2O_3 in terms of new low wavenumber features and a prominent A_{1g} breathing mode. Series C experiments demonstrate the limit of the dilute precursor condition for full oxidation to MnO_2. Oxygen-lean conditions were also examined to observe the formation of lower manganese oxidation states in series D experiments. Flames having $1.2 < \phi < 1.5$ were studied and the summary is shown in Fig. 7. As the computed oxygen profiles shows, manganese oxide forms under similar flame structure with oxygen being the only variation across the flames. The formation of MnO is observed for the first time by flame synthesis. The XRD and Raman features show a systematic evolution from Mn_3O_4 products to MnO products at the equivalence ratio is increased (gas-phase O_2 decreases). A range of titanium oxide structures was reported for increasing equivalence ratio [13] but a range of metal oxide valence this extensive has not been observed. Experiment C and D demonstrate the manipulation of O_2 during particle growth to systematically control the resulting particle oxidation state / structure. The premixed stagnation flame configuration enables systematic study of competing oxidation and growth processes. The current work demonstrates approaches to design nanoparticle properties and potentially extract fundamental synthesis parameters such as oxidation rate.

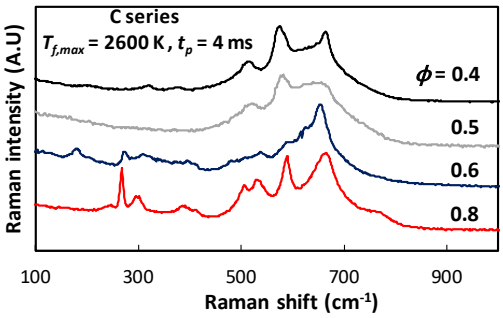

Figure 6. Raman spectra measured for the experiment C series of flames ($0.4 < \phi < 0.8$)

.

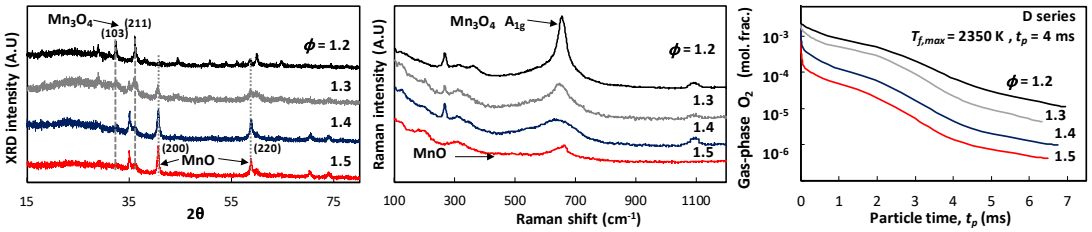

Figure 7. Summary of manganese oxides formed in experiment D series of flames (1.2 < ϕ < 1.5). XRD patterns for increasing equivalence ratio (left panel). Also shown are Raman spectra (middle panel) and computed (OPPDIF) oxygen-time history (right panel) for the series.

5. Conclusion

The variation in manganese oxidation state in the products observed here is shown to be caused by competing oxidation and particle nucleation processes. Complimentary experimental and modeling studies of flame synthesis were carried out under well-defined boundary conditions to examine this competition. The pseudo 1D formulation used by OPPDIF to calculate the flame structure performs reasonably well for the narrow aspect ratio stagnation flow currently studied. Unlike iron oxide and titanium oxide systems, complete oxidation to MnO_2 is only observed for the most oxidizing growth conditions. Manipulation of the balance between manganese oxidation and particle nucleation through control of the time-temperature-oxygen history may enable selective synthesis of manganese oxide nanoparticles with tailored morphology and oxidation state.

6. Acknowledgments

The work was supported NSF Combustion and Fire Systems program under Award 1841357. Prof. David Pullman (SDSU Chemistry) and Dr. Ingrid Neisman (SDSU Microscopy Center) are gratefully acknowledged for assistance in nanoparticle characterization.

References

[1] C. K. Law, Combustion Physics. Cambridge: Cambrige Press, 2006.

[2] U. Niemann, K. Seshadri, F. A. Williams, Accuracies of laminar counterflow flame experiments, Combust. Flame 162, (4)(2015) 1540–1549.

[3] C. K. Law, F. Wu, F. N. Egolfopoulos, V. Gururajan, H. Wang, On the Rational Interpretation of Data on Laminar Flame Speeds and Ignition Delay Times, Combust. Sci. Technol. 187 (1–2)(2015) 27–36.

[4] E. Meeks, R. J. Kee, D. S. Dandy, M. E. Coltrin, Computational simulation of diamond chemical vapor deposition in premixed C2H2/O2/H2 and CH4O2-strained flames, Combust. Flame 92 (1)(1993) 144–160

[5] N. G. Glumac D. G. Goodwin, Large-area diamond film growth in a low-pressure flame, Mater. Lett. 18

(3)(1993) 119–122.
[6] W. Wei, X. Cui, W. Chen, D. G. Ivey, Manganese oxide-based materials as electrochemical supercapacitor electrodes, Chem. Soc. Rev. 40 (3)(2011) 1697–1721.
[7] M. M. Thackeray, C. S. Johnson, J. T. Vaughey, N. Li, S. A. Hackney, Advances in manganese-oxide 'composite' electrodes for lithium-ion batteries, J. Mater. Chem. 15 (23)(2005) 2257–2267.
[8] M. Kang, E. D. Park, J. M. Kim, J. E. Yie, Manganese oxide catalysts for NOx reduction with NH3 at low temperatures, Appl. Catal. A Gen. 327 (2)(2007) 261–269.
[9] M. Wiechen, M. M. Najafpour, S. I. Allakhverdiev, L. Spiccia, Water oxidation catalysis by manganese oxides: learning from evolution, Energy Environ. Sci. 7 (7) (2014) 2203–2212.
[10] F. O. Ernst, H. K. Kammler, A. Roessler, S. E. Pratsinis, W.J. Stark, J. Ufheil, P. Novak, Electrochemically active flame-made nanosized spinels: LiMn2O4, Li4Ti5O12 and LiFe5O8, Mater. Chem. Phys. 101 (2-3)(2007) 372–378.
[11] S. Li, Y. Ren, P. Biswas, S. D. Tse, Flame aerosol synthesis of nanostructured materials and functional devices: Processing, modeling, and diagnostics, Prog. Energy Combust. Sci. 55 (2016) 1–59.
[12] J. Camacho, C. Liu, N. Montes, H. Wang, Ultrafine Manganese Oxide Nanoparticles Synthesized by Flame Stabilized on a Rotating Surface, 9th U. S. Natl. Combust. Meet., 2015, 2B09.
[13] M. Y. Manuputty, J. A. H. Dreyer, Y. Sheng, E. J. Bringley, M. L. Botero, J. Akroyd, M. Kraft, Polymorphism of nanocrystalline TiO2 prepared in a stagnation flame: formation of the TiO2-II phase, Chem. Sci., 10 (2019) 1342-1350 .
[14] K. Seshadri, F. A. Williams, Laminar flow between parallel plates with injection of a reactant at high reynolds number, Int. J. Heat Mass Transf. 21 (2)(1978) 251–253.
[15] J. M. Bergthorson, S. D. Salusbury, P. E. Dimotakis, Experiments and modelling of premixed laminar stagnation flame hydrodynamics, J. Fluid Mech. 681 (2011) 340–369.
[16] C. Houtman, D. B. Graves, K. F. Jensen, CVD in Stagnation Point Flow: An Evaluation of the Classical 1D Treatment , J. Electrochem. Soc. 133 (5) (1986) 961–970.
[17] A. E. Lutz, R. J. Kee, J. F. Grcar, F. M. Rupley, OPPDIF: A Fortan program for computing opposed-flow diffusion flames, Report No. SAND-96-8243, Sandia National Labs, Livermore, 1997.
[18] A. D. Abid, J. Camacho, D. A. Sheen, H. Wang, Quantitative measurement of soot particle size distribution in premixed flames - The burner-stabilized stagnation flame approach, Combust. Flame, 156 (10) (2009) 1862–1870.
[19] R. J. Kee, F. M. Rupley, J. A. Miller, Chemkin-II: A Fortran chemical kinetics package for the analysis of gas-phase chemical kinetics. report No. SAND90-8003B, Sandia National Labs, Livermore, 1989.
[20] H. Wang, X. You, A. V. Joshi, S. G. Davis, A. Laskin, F. Egolfopoulos, C. K. Law, USC Mech II. High-Temperature Combustion Reaction Model of H2/CO/C1-C4 Compounds, http://ignis.usc.edu/USC_Mech_II.htm, 2007.
[21] J. Camacho, A. V. Singh, W. Wang, R. Shan, E. K. Y. Yapp, D. Chen, M. Kraft, H. Wang, Soot particle size distributions in premixed stretch-stabilized flat ethylene-oxygen-argon flames, Proc. Combust. Inst. 36 (2017) (1001-1009).
[22] E. K. Y. Yapp, D. Chen, J. Akroyd, S. Mosbach, M. Kraft, J. Camacho, H. Wang, Numerical simulation and parametric sensitivity study of particle size distributions in a burner-stabilised stagnation flame, Combust. Flame, 162 (6) (2015) 2569-2581.
[23] J. Bonpua, Y. Yagües, A. Aleshin, S. Dasappa, J. Camacho, Flame temperature effect on sp^2 bonds on nascent carbon nanoparticles formed in premixed flames ($T_{f,max}$ > 2100 K): A Raman spectroscopy and particle mobility sizing study, Proc. Combust. Inst., 37 (1)(2019) 943–951, 2019.
[24] J. M. Bergthorson, *Experiments and Modeling of Impinging Jets and Premixed Hydrocarbon Stagnation Flames*, PhD thesis, California Institute of Technology, Pasadena, California, USA, 2005.
[25] V. Mittal, H. Pitsch, F. Egolfopoulos, Assessment of counterflow to measure laminar burning velocities using direct numerical simulations, Combust. Theory Model., 16 (3)(2012) 419–433.
[26] R. F. Johnson, A. C. VanDine, G. L. Esposito, H. K. Chelliah, On the Axisymmetric Counterflow Flame Simulations: Is There an Optimal Nozzle Diameter and Separation Distance to Apply Quasi One-Dimensional Theory?, Combust. Sci. Technol., 187 (1–2) (2015) 37–59.
[27] T. Yuan, Y.-H. Lai, C.-K. Chang, Numerical studies of heterogeneous reaction in stagnation flows using one-dimensional and two-dimensional Cartesian models, Combust. Flame, 154, (3)(2008) 557–568.
[28] N. Bouvet, D. Davidenko, C. Chauveau, L. Pillier, Y. Yoon, On the simulation of laminar strained flames in

stagnation flows: 1D and 2D approaches versus experiments, Combust. Flame, 161 (2)(2014) 438–452.
[29] F. Buciuman, F. Patcas, R. Craciun, D. R. T. Zahn, D. R. T. Zahn, Vibrational spectroscopy of bulk and supported manganese oxides, Phys. Chem. Chem. Phys., 1 (1)(1999) 185–190.
[30] C. Julien, M. Massot, S. Rangan, M. Lemal, D. Guyomard, Study of structural defects in γ-MnO2 by Raman spectroscopy, J. Raman Spectrosc., 33 (4)(2002) 223–228.

List of Figures

List of Supplemental Material (available upon request jcamacho@sdsu.edu)

Table S.1 Detailed flame conditions.

Figure S.1 Comparison of measured flame position between MMT doped flames and base flames without doping for B5-B8.